Thermal decoupling in high-T_c cuprate superconductors

Sungwoo Lee[1,2]*, Woojin Choi[1], Youngje Kim[1], Young-Kyun Kwon[3], Dongjoon Song[4], Miyoung Kim[1,2],

Gun-Do Lee[1,2]*

[1]Department of Material Science and Engineering, Seoul National University, Seoul, Korea

[2]Institute of Advanced Materials Seoul National University Seoul 08826, Republic of Korea

[3]Department of Physics, Department of Information Display, and Research Institute for Basic Sciences, Kyung Hee University, Seoul, 02447, Korea

[4]Stewart Blusson Quantum Matter Institute, University of British Columbia, Vancouver, British Columbia V6T 1Z1, Canada

*corresponding authors: gdlee@snu.ac.kr, blessing1223@gmail.com

RECEIVED DATE

Abstract

Although many years have passed since the discovery of high-critical-temperature (high-T_c) superconducting materials[1,2], the underlying mechanism is still unknown. The B_{1g} phonon anomaly in high-T_c cuprate superconductors has long been studied[3-5]; however, the correlation between the B_{1g} phonon anomaly and superconductivity has yet to be clarified. In the present study, we successfully reproduced the B_{1g} phonon anomaly in YBa$_2$Cu$_3$O$_7$ (YBCO) using an *ab initio* molecular dynamics (AIMD) simulation and temperature-dependent effective potential (TDEP) method. The A_g phonon by Ba atoms shows a more severe anomaly than the B_{1g} phonon at low temperatures. Our analysis of the phonon anomaly and the temperature-dependent phonon

dispersion indicated that decoupling between thermal phenomena and electron transport at low temperatures leads to layer-by-layer thermal decoupling in YBCO. Electronically and thermally isolated Ba atoms in YBCO are responsible for the thermal decoupling. The analytic study of the thermal dcoupling revealed that Planckian dissipation[6,7] expressing linear-T resistivity is another expression of the Fermi liquid of the CuO$_2$ plane. The Uemura plot [8,9] of the relationship between T_c and the Fermi temperature, as well as the superconducting dome in YBCO, is explained rigorously and quantitatively. Our findings not only present a new paradigm for understanding high-T_c superconductivity but also imply that the spontaneous formation of low-temperature layers in materials can lead to revolutionary changes in the thermal issues of industrial fields.

Main

The most important issue in the study of unconventional superconductivity involves the proposed mechanism, which seems to explain superconductivity but does not fit well when applied to newly discovered high-critical-temperature (high-T_c) superconducting materials. Recently, many superconductors have been discovered due to the explosive increase in low-temperature-physics research[10-16], and more theories have been proposed as the superconducting materials to be applied have become more diversified[17-22]. It is generally accepted that the electron–phonon interaction in the Bardeen–Cooper–Schrieffer (BCS) theory[18,23] is still important and that this basic mechanism governing superconductivity does not change. Therefore, most research has been performed using the concept that high-T_c superconductivity is induced by strong electron–phonon interaction[24-27]. In the process, many studies have focused on elucidating the states of electrons and their strong correlations in high-T_c superconductors[28-30]. However, despite the importance of phonons in the electron-phonon interaction, phonons have not been as well studied as electrons in unconventional superconductivity. Notably, a recent angle-resolved photoemission spectroscopy study indicated the necessity for B$_{1g}$ phonon investigation in relation to the importance of electron–phonon coupling, as the system evolves from the BCS regime to

the high-T_c regime in heavily over-doped Bi2212[31]. It has been also reported that phonons play an important role in pseudogap phase of cuprates [32].

A phonon anomaly is a representative phonon phenomenon that appears peculiarly in high-T_c cuprate superconductors[3,26,33]. Numerous studies have been conducted on phonon anomalies as they relate to superconductivity. In particular, the B_{1g} phonon anomaly of YBCO appears just above T_c when the temperature is lowered, and the B_{1g} phonon frequency drops rapidly due to softening below T_c[3-5]. The B_{1g} phonon anomaly is believed to originate from the depletion of the electron density of states due to the gap opening[31]; however, the relationship between the two has not been resolved. A better understanding of the B_{1g} phonon anomaly and an explanation of its consequences regarding superconductivity are necessary.

In this study, we investigated the phonon anomaly in YBCO using the *ab initio* molecular dynamics (AIMD) simulation method and the temperature-dependent effective potential (TDEP) method[34,35]. First, we performed constant temperature AIMD at various temperatures. The TDEP method can extract the force constant from the AIMD results and is useful for temperature-dependent phonon studies including anharmonic effects[36]. Notably, ours is the first simulation report on the B_{1g} phonon anomaly. Beyond the confirmation of the B_{1g} phonon anomaly, we also revealed thermal decoupling inside YBCO that is induced due to the decoupling between the thermal properties and electron transport. Based on our analysis, we demonstrate that this thermal decoupling is an important key to understanding high-T_c superconductivity.

Results

We performed AIMD simulations at various temperatures, decreasing from 300 to 20 K, and obtained temperature-dependent phonon dispersions using the TDEP method. Figure 1a shows the frequency of the B_{1g} phonon as a function of temperature. The B_{1g} phonon mode is the out-of-plane vibration mode of oxygen atoms in the CuO_2 plane. Our simulation shows that the frequency of the B_{1g} phonon increases as

the temperature decreases from 300 to 150 K, with a more gradual decrease around 150 K, similar to the behavior observed in experiments[3-5]; however, the frequency drops abruptly near 70 K, which is slightly different from what was observed experimentally, in which the B_{1g} phonon frequency drops abruptly near the superconducting temperature, at ~90 K. We will discuss this difference later in our analysis. Intriguingly, this anomalous behavior occurs not only in the B_{1g} phonon but also in the A_g phonon, which is even stronger, as shown in Fig. 1b. The A_g phonon is an out-of-plane mode mainly from Ba atoms. The frequency of the A_g phonon decreases by ~70 cm^{-1} from 300 to 20 K, whereas that of the B_{1g} phonon decreases by just 1.3 cm^{-1}. Such an A_g phonon anomaly originating from Ba atoms has been reported in Raman spectroscopy for YBCO[37]. However, no serious anomaly has been reported, which could be due to the thermalization associated with spectroscopy measurements. Phonons with low frequencies are generally affected by observation processes such as those involving lasers[38]. Notably, many other out-of-plane phonons, as well as the B_{1g} and A_g phonons, are softened when the temperature is reduced below T_c (Supplementary Fig. 1), which has also been observed in Raman spectroscopy [39].

To investigate the effect of phonon softening on the thermodynamics of YBCO, we analyzed the phonon dispersion relation with respect to temperature. Figure 2a shows phonon dispersions obtained from TDEP calculations carried out after AIMD simulations at 300, 90, and 30 K. The internal energy of a harmonic crystal is given by the following[40]:

$$U = Vu^{\mathrm{eq}} + \sum_{\mathbf{k}s} \frac{1}{2}\hbar\omega_s(\mathbf{k}) + \sum_{\mathbf{k}s} \frac{\hbar\omega_s(\mathbf{k})}{e^{\beta\hbar\omega_s(\mathbf{k})} - 1} \ , \tag{1}$$

where V is the crystal volume, $\omega_s(\mathbf{k})$ is the frequency of the phonon modes, and β is $1/k_BT$. The first and second terms represent the energy of the equilibrium configuration and the energy of zero point vibration, respectively. The last term is the temperature-dependent part of the internal energy (TDPIE), of which the frequency dependence is displayed as the background color of Fig. 2a. The contribution of Ba atoms for each phonon mode and the wave vector are also calculated from the phonon eigenstates, which is shown as the grayscale lines overlaying the phonon dispersion curves in Fig. 2a. The contribution

of Ba atoms for each phonon mode is distributed mainly in the low-frequency phonon modes; this contribution does not change significantly as the temperature decreases. This implies that the contribution ratio of Ba atoms to TDPIE increases as the contribution of high-frequency phonons to TDPIE decreases with the temperature. Figure 2b shows the contribution of each type of atom to TDPIE as a function of temperature. The contribution of Ba atoms to TDPIE increases as the temperature decreases, reaching a maximum near 30 K. Thus, the contribution of each type of atom to the internal energy is different at low temperatures. As such, this behavior is expected to affect the thermal properties of YBCO, potentially generating local thermal phenomena at low temperature, depending on the type of atom.

It is well known that free electrons in metals play an important role in thermal transport and are capable of delocalizing local thermal phenomena. Figure 2c shows the charge density distribution in YBCO, which reveals that the Ba atom is separated electronically from the other atoms, especially from the Cu and O atoms in the CuO_2 plane below. This result indicates that the thermal properties in YBCO due to the specific thermal phenomena that emerged from Ba atoms can be separated from the electronic properties determined by the CuO_2 plane. It has been reported that the non-equilibrium steady state is sustained and the Wiedemann–Franz law could break down when heat and particle flow are decoupled or weakly coupled at low temperatures[41]. The deep softening of the out-of-plane phonons from Ba atoms and O atoms of the CuO_2 plane due to the B_{1g} and A_g phonon anomalies indicates bond weakening between the two that sharply reduces the thermal transport, resulting in the thermal decoupling between the Ba atom and CuO_2 plane.

To explore further the thermal decoupling in YBCO, we calculated the kinetic energy from the velocity of atoms at each time step of the AIMD simulation and extracted layer-by-layer temperatures from the kinetic energy-temperature relation ($\frac{1}{2}mv^2 = \frac{3}{2}k_B T$). Because the temperature is extracted theoretically and intentionally, we refer to it as the 'extracted temperature' (T_{ext}) to distinguish it from the real temperature measured in experiments. Figures 3a, 3b, and 3c show the T_{ext}s of the BaO plane, CuO_2 plane, Y layer, and CuO chain at the simulation temperatures of 300, 90, and 30 K, respectively. At 300 K,

almost all layers have the same T_{ext}, whereas, at the simulation temperatures of 90 and 30 K, the T_{ext} of the BaO plane is higher than those of the other planes. Our results indicate that the high T_{ext} of the BaO plane is mainly due to the Ba atoms, as shown in Figs. 3e and 3f. This is consistent with our analysis of the temperature-dependent phonon dispersion shown in Fig. 2b.

Application to Unconventional Superconductor Mysteries and Experimental Evidence

The question is then whether this thermal decoupling can be observed experimentally. It has been reported that the surface of YBCO is stabilized mainly with the termination of the BaO plane[42]. The stability of the BaO surface from our AIMD simulation is also discussed in Supplementary Discussion 1. In the AIMD simulation, the BaO surface acts as a protective surface layer for YBCO. Therefore, the measured temperature in experiments is likely to coincide with the temperature of the BaO surface. As such, we attempted to scale the system temperature to the T_{ext} of the BaO plane to re-analyze the B_{1g} phonon anomaly curve shown in Fig. 1a. The B_{1g} phonon anomaly depending on T_{ext} of the BaO plane is shown in Fig. 4a; notably, the experimental observations exhibited an abrupt drop in the B_{1g} phonon curve near the superconducting temperature (~90 K). This result suggests that the measured temperature in the experiment could be the T_{ext} of the BaO plane. We also attempted to clarify the relationship between the T_{ext} of the surface BaO plane (T_{BaO}) and the T_{ext} of the conducting CuO_2 plane (T_{CuO_2}) from our AIMD simulation in Fig. 4b. From the optimally fitted curve for the normal state at $T_{BaO} > 100$ K, as shown in Fig. 4b, we found that the two temperatures are coupled to $T_{BaO} = 2.08 \times 10^{-3} \, T_{CuO_2}^{2.02} + 108.2$. Because the fitting equation satisfies essentially the quadratic relation of $T_{BaO} \propto T_{CuO_2}^{2}$, we refitted their relationship quadratically to obtain $T_{BaO} = 2.31 \times 10^{-3} \, T_{CuO_2}^{2} + 107.6$. We defined the decoupling temperature, T_{dec}, below which the thermal decoupling occurs between the two planes, as the temperature at which the slope of the quadratic fitting curve becomes one, implying that T_{BaO} and T_{CuO_2} approach the same value. This value was estimated to be $T_{dec} = 216.3$ K from our AIMD simulation results, as shown

in Fig. 4b. Here, we demonstrate that this thermal decoupling is the origin of the famous phenomenological formula in high-T_c cuprate superconductivity, i.e. the Planckian dissipation[6,7]:

$$\frac{\hbar}{\tau} = \alpha k_B T, \tag{2}$$

where τ, α, and T are the relaxation time, a dimensionless parameter, and the measured temperature, respectively, and $\hbar$ and k_B are Planck's and Boltzmann's constant, respectively. The Planckian dissipation expresses the linear-T resistivity behavior in the strange metal phase of the cuprates. However, the origin of the Planckian dissipation has not been understood until now. τ should be determined by the conducting CuO_2 plane. Since the stable surface of YBCO is the BaO plane, the measured temperature T in experiments can be regarded as T_{BaO}. By replacing T by the quadratic fitting formula in the Planckian dissipation (2), we obtained $\hbar/\tau \propto 2.31 \times 10^{-3} \, T_{CuO_2}^2$, indicating that the Planckian dissipation can be expressed like a Fermi liquid, as a quadratic term of T_{CuO_2}. Therefore, the general resistivity form of the Fermi liquid for the CuO_2 plane is given by

$$\rho_{Fermi} = A \frac{k_B T_{CuO_2}^2}{\hbar T_F} \frac{m^*}{ne^2}, \tag{3}$$

where A is a dimensionless parameter from the Fermi liquid; and T_F, m^*, and n are the Fermi temperature, the effective mass, and the carrier concentration, respectively. The resistivity will follow ρ_{Fermi} above T_{dec}, because T_{CuO_2} is the same as T_{BaO} as well as the measured temperature. However, below T_{dec}, the measured temperature is expressed as T_{BaO} and the resistivity will follow Planckian dissipation:

$$\rho_{Planckian} = \alpha \frac{k_B T_{BaO}}{\hbar} \frac{m^*}{ne^2}. \tag{4}$$

Here, we consider the superconducting critical temperature of the CuO_2 plane as T_0. The superconducting temperature (T_c) for the BaO plane will differ, depending on T_{dec}, as shown in Supplementary Figs. 3 and 4. The resistivity and the derivatives of Eqs. (3) and (4) should be the same at T_{dec}. For the relation, we

obtain $T_{\text{dec}} = \frac{\alpha}{2A} T_F$; the superconducting critical temperature, T_c, is derived from the following (see Supplementary Discussion 2 for the detailed derivation):

$$T_c = \frac{A\,T_0^{\,2}}{\alpha\,T_F} + \frac{\alpha}{4A}T_F \tag{5}$$

$$\approx \frac{\alpha}{4A}T_F, \tag{6}$$

where the approximation comes from $T_F \gg T_0$. This result explains the linear relationship between T_c and T_F from the Uemura plot[8,9]. We compare the linear coefficient to corroborate more clearly the linear relation from the Uemura plot. Given that T_{dec} was calculated to be 216.3 K from our simulation results and T_F is about 2450 K [43] for YBa$_2$Cu$_3$O$_7$, we estimated $A = 5.67$ with $\alpha \approx 1$ for almost all cuprates[44]. The coefficient A, which is the parameter from Fermi liquid resistivity in Eq. (3), is generally taken to be of an order unity within one power of ten[40], indicating that the resistivity of the CuO$_2$ plane is in good agreement with that of the general Fermi liquid. From Eq. (6), we found $T_c/T_F = 0.044$, which is in excellent agreement with $T_c/T_F = 0.042$ for cuprates from the Uemura plot[9] (See also Supplementary Fig. 5). In Supplementary Discussion 3, we describe in more detail the relationship between T_c and T_F and explain the resulting Uemura plot for overdoped cuprates. In our study, we found that the two representative mysteries in unconventional high-T_c superconductivity, specifically, the linear-T resistivity and the Uemura plot, are closely connected and can be explained by the thermal decoupling.

We also revealed a relationship between the thermal decoupling and the superconducting temperature considering the distance between the Ba atom and CuO$_2$ plane. Even though, as mentioned, the Ba atom and CuO$_2$ plane are separated from each other electronically and thermally, a reduction in the distance between the two induces the thermalization of the CuO$_2$ plane, which affects T_c. The doping concentration in high T_c superconductors is a known key factor in determining T_c. However, their relationship has not been clearly resolved. The doping concentration affects the structure of YBCO and is determined by the number of oxygen atoms in the YBCO unit cell. As the number of oxygen atoms increases from $x = 6$ to

7 in $YBa_2Cu_3O_x$, the cell size c along the z-direction becomes shorter. However, it is very intriguing that the Ba-CuO_2 plane distance becomes longer whereas the cell size c becomes shorter[45-47]. From our results, we can conjecture that the change in distance between the Ba and CuO_2 planes affects T_c. Surprisingly, Fig. 5a shows that the variation of T_c is well-matched with the Ba-CuO_2 plane distance modulated by the doping concentration. Therefore, we need to consider superconducting phenomena from the viewpoint of thermal decoupling. In cuprates replaced by Sr instead of Ba, Sr could play the same role as Ba, as it is also an alkali earth metal on the neighboring layer of the CuO_2 plane in Sr-doped cuprates. In our study expanded to other cuprate superconductors containing Ba and Sr, we also found that the distance between Ba or Sr and the CuO_2 plane is closely related to the enhancement of T_c[48-57]. Figure 5b shows the relationship between T_c and the distance between Ba or Sr and the CuO_2 plane in various cuprates. Among cuprates having a similar composition, T_c increases with the distance, implying an enhancement in the thermal decoupling. Especially, in the case of the Hg-Ba-Ca-Cu-O compound, T_c is closely related to the distance between Ba and the CuO_2 plane, regardless of the trend in the composition ratio.

Discussion

Here, we can extract T_0 (superconducting temperature of CuO_2 plane) for underdoped cuprates superconductors where the thermal decoupling is well applied from the least square fitting of experimental data for eq. (5) as shown in Supplementary Fig. 6. We found that T_0 is about 14 K which is in excellent agreement with the lowest T_c reported in YBCO [58]. This value is within the limit of BCS theory. Therefore, we may explain the unconventional high-T_c superconductivity in the framework of BCS theory. From our results, heavy elements like Ba play the role of a heat absorber due to the low-frequency phonons from those elements in phonon dispersion, which is important to the enhancement of T_c. The high pressure-induced superconductivity from hydrides is a good example of the combination of heavy and light elements. It has been reported that the combination of heavy and light elements could generate many-body localized states from quantum disentanglement[59]. Many-body localization is a dynamic phenomenon occurring in isolated many-body quantum systems that are characterized by non-equilibrium states. The

decoupling between the thermal property and electron transport and the resulting thermal decoupling in cuprates can be treated as non-equilibrium thermodynamic states embodying the phase transition from volume law entanglement to area law entanglement at low temperature [60]. It may also be related to Bekenstein and Hawking's black hole physics regarding the area law of entropy on the black hole horizon[61,62]. It would be interesting to study the relationship between this thermal decoupling and many-body localization. Thermal decoupling may tell us of the necessity of modifying the measured temperature. In the experiment, careful speculation is also needed, as the temperature coinciding with important physical properties can be different from the measured temperature. Above all, the most important result from our study is that a low-temperature layer relative to the surface layer can be generated spontaneously in solids, despite the lesser effort required for cryogenics. This may provide a unique means of solving frequently confronted thermal problems associated with quantum devices, quantum computing, and information transfer.

Methods

***Ab initio* molecular dynamics (AIMD) simulation and the temperature-dependent effective potential (TDEP) method**

We performed AIMD simulations using the Vienna *ab initio* simulation package (VASP) code[63,64] with a Nosé–Hoover thermostat[65,66] controlling the temperature. Plane-wave pseudopotential calculations using ultrasoft pseudopotentials[67] were carried out within the framework of the generalized gradient approximation of the Perdew–Burke–Ernzerhof functional[68]. The energy cut-off for the plane-wave basis was set to 400 eV. The DFT-D3 scheme proposed by Grimme et al.[69] was used to approximate the long-range dispersion forces. In this simulation, we adopted a $4\times4\times1$ bulk supercell and one Γ point for k-point sampling in the Brillouin zone. All AIMD simulations were performed with a time step of 1 fs within the *NVT* ensemble. After we first performed an AIMD simulation at 300 K for over 60 ps, we continued AIMD simulations at each temperature for 60 ps by decreasing the temperature by 10 K for 5 ps from 300

to 20 K. To obtain the phonon properties of YBCO, the effective force constant matrices were calculated using the TDEP code[34,35] with atomic displacements and forces from the AIMD at finite temperatures; this process was carried out by least-squares fitting of AIMD displacements and forces to the crystal model Hamiltonian. We rigorously tested the convergence of the phonon properties of YBCO in the TDEP calculations.

In the simulation, we adopted the orthorhombic structure of $YBa_2Cu_3O_7$ (15.308 Å×15.652 Å×11.738 Å) that was extended by 0.08 Å along the c-axis compared to the *ab initio* optimized structure. In the simulation, we found that the phonon frequency of the *ab initio* optimized structure was overestimated, which is related to a general tendency to overestimate the bulk modulus in *ab initio* calculations. Therefore, we performed TDEP calculations from AIMD results on the structure, in which the lattice constant was extended along the *c*-axis; the results were in good agreement with the experimental results of the B_{1g} phonon frequency, as shown in Fig. 1a. To check the robustness of our results, we also performed AIMD simulations and TDEP calculations for the *ab initio* optimized structure, and obtained similar phonon anomalies to those of Fig. 1 and layer-by-layer thermal decoupling (Supplementary Fig. 7).

Author contributions

G.-D.L. and S.L. conceived the project and performed simulations. W.C. and Y.K. collected supporting experimental data. Y.-K.K., D.S., and M.K. advised on the project, and G-.D.L, S.L., Y.-K.K., and D.S. wrote the manuscript. All of the authors discussed and commented on the manuscript.

Additional information

Supplementary information is available in the online version of the paper. Correspondence and requests for materials should be addressed to G.-D.L. and S.L..

Competing financial interests

The authors declare no competing financial interests.

References

1 Bednorz, J. G. & Müller, K. A. Possible high T_c superconductivity in the Ba−La−Cu−O system. *Zeitschrift für Physik B Condensed Matter* **64**, 189-193, doi:10.1007/BF01303701 (1986).

2 Wu, M. K. *et al.* Superconductivity at 93 K in a new mixed-phase Y-Ba-Cu-O compound system at ambient pressure. *Physical Review Letters* **58**, 908-910, doi:10.1103/PhysRevLett.58.908 (1987).

3 Driza, N. *et al.* Long-range transfer of electron–phonon coupling in oxide superlattices. *Nature Materials* **11**, 675-681, doi:10.1038/nmat3378 (2012).

4 Altendorf, E., Chen, X. K., Irwin, J. C., Liang, R. & Hardy, W. N. Temperature dependences of the 340-, 440-, and 500-cm^{-1} Raman modes of $YBa_2Cu_3O_y$ for $6.7 \lesssim y \lesssim 7.0$. *Physical Review B* **47**, 8140-8150, doi:10.1103/PhysRevB.47.8140 (1993).

5 Oh, D. *et al.* B_{1g}-Phonon Anomaly Driven by Fermi Surface Instability at Intermediate Temperature in $YBa_2Cu_3O_{7-\delta}$. *Physical Review Letters* **127**, 277001, doi:10.1103/PhysRevLett.127.277001 (2021).

6 Zaanen, J. Why the temperature is high. *Nature* **430**, 512-513, doi:10.1038/430512a (2004).

7   Zaanen, J. Planckian dissipation, minimal viscosity and the transport in cuprate strange metals. *Scipost Physics* **6**, doi:10.21468/SciPostPhys.6.5.061 (2019).

8   Uemura, Y. J. *et al.* Basic similarities among cuprate, bismuthate, organic, Chevrel-phase, and heavy-fermion superconductors shown by penetration-depth measurements. *Physical Review Letters* **66**, 2665-2668, doi:10.1103/PhysRevLett.66.2665 (1991).

9   Hashimoto, K. *et al.* A Sharp Peak of the Zero-Temperature Penetration Depth at Optimal Composition in $BaFe_2(As_{1-x}P_x)_2$. *Science* **336**, 1554-1557, doi:doi:10.1126/science.1219821 (2012).

10   Ge, J.-F. *et al.* Superconductivity above 100 K in single-layer FeSe films on doped $SrTiO_3$. *Nature Materials* **14**, 285-289, doi:10.1038/nmat4153 (2015).

11   Zhao, H. *et al.* Cascade of correlated electron states in the kagome superconductor CsV_3Sb_5. *Nature* **599**, 216-221, doi:10.1038/s41586-021-03946-w (2021).

12   Jiao, L. *et al.* Chiral superconductivity in heavy-fermion metal UTe_2. *Nature* **579**, 523-527, doi:10.1038/s41586-020-2122-2 (2020).

13   Kamihara, Y. *et al.* Iron-Based Layered Superconductor: LaOFeP. *Journal of the American Chemical Society* **128**, 10012-10013, doi:10.1021/ja063355c (2006).

14   Li, D. *et al.* Superconductivity in an infinite-layer nickelate. *Nature* **572**, 624-627, doi:10.1038/s41586-019-1496-5 (2019).

15   Chen, Z. *et al.* Electric field control of superconductivity at the $LaAlO_3$/$KTaO_3$(111) interface. *Science* **372**, 721-724, doi:doi:10.1126/science.abb3848 (2021).

16   Cao, Y. *et al.* Unconventional superconductivity in magic-angle graphene superlattices. *Nature* **556**, 43-50, doi:10.1038/nature26160 (2018).

17   Fröhlich, H. On the theory of superconductivity: the one-dimensional case. *Proceedings of the Royal Society of London. Series A. Mathematical and Physical Sciences* **223**, 296-305, doi:doi:10.1098/rspa.1954.0116 (1954).

18   Bardeen, J., Cooper, L. N. & Schrieffer, J. R. Microscopic Theory of Superconductivity. *Physical Review* **106**, 162-164, doi:10.1103/PhysRev.106.162 (1957).

19   Borzi, R. A. *et al.* Formation of a Nematic Fluid at High Fields in $Sr_3Ru_2O_7$. *Science* **315**, 214-217, doi:doi:10.1126/science.1134796 (2007).

20   Kargarian, M., Efimkin, D. K. & Galitski, V. Amperean Pairing at the Surface of Topological Insulators. *Physical Review Letters* **117**, 076806, doi:10.1103/PhysRevLett.117.076806 (2016).

21   Wu, F., MacDonald, A. H. & Martin, I. Theory of Phonon-Mediated Superconductivity in Twisted Bilayer Graphene. *Physical Review Letters* **121**, 257001, doi:10.1103/PhysRevLett.121.257001 (2018).

22   Lian, B., Wang, Z. & Bernevig, B. A. Twisted Bilayer Graphene: A Phonon-Driven Superconductor. *Physical Review Letters* **122**, 257002, doi:10.1103/PhysRevLett.122.257002 (2019).

23   Bardeen, J., Cooper, L. N. & Schrieffer, J. R. Theory of Superconductivity. *Physical Review* **108**, 1175-1204, doi:10.1103/PhysRev.108.1175 (1957).

24   Lanzara, A. *et al.* Evidence for ubiquitous strong electron–phonon coupling in high-temperature superconductors. *Nature* **412**, 510-514, doi:10.1038/35087518 (2001).

25   Timusk, T., Porter, C. D. & Tanner, D. B. Strong electron-phonon interaction in the high-T_c superconductors: Evidence from the infrared. *Physical Review Letters* **66**, 663-666, doi:10.1103/PhysRevLett.66.663 (1991).

26   Le Tacon, M. *et al.* Inelastic X-ray scattering in $YBa_2Cu_3O_{6.6}$ reveals giant phonon anomalies and elastic central peak due to charge-density-wave formation. *Nature Physics* **10**, 52-58, doi:10.1038/nphys2805 (2014).

27   Egami, T. *et al.* Electron–phonon interactions in HTSC cuprates. *Physica B: Condensed Matter* **316-317**, 62-68, doi:https://doi.org/10.1016/S0921-4526(02)00426-X (2002).

28   Tokura, Y. & Nagaosa, N. Orbital Physics in Transition-Metal Oxides. *Science* **288**, 462-468, doi:doi:10.1126/science.288.5465.462 (2000).

29   Corson, J., Mallozzi, R., Orenstein, J., Eckstein, J. N. & Bozovic, I. Vanishing of phase coherence in underdoped $Bi_2Sr_2CaCu_2O_{8+\delta}$. *Nature* **398**, 221-223, doi:10.1038/18402 (1999).

30   Iguchi, I., Yamaguchi, T. & Sugimoto, A. Diamagnetic activity above T_c as a precursor to superconductivity in $La_{2-x}Sr_xCuO_4$ thin films. *Nature* **412**, 420-423, doi:10.1038/35086540 (2001).

31   He, Y. *et al.* Rapid change of superconductivity and electron-phonon coupling through critical doping in Bi-2212. *Science* **362**, 62-65, doi:doi:10.1126/science.aar3394 (2018).

32   Grissonnanche, G. *et al.* Chiral phonons in the pseudogap phase of cuprates. *Nature Physics* **16**, 1108-1111, doi:10.1038/s41567-020-0965-y (2020).

33   Bakr, M. *et al.* Electronic and phononic Raman scattering in detwinned $YBa_2Cu_3O_{6.95}$ and $Y_{0.85}Ca_{0.15}Ba_2Cu_3O_{6.95}$: *s*-wave admixture to the d_{x2-y2}-wave order parameter. *Physical Review B* **80**, 064505, doi:10.1103/PhysRevB.80.064505 (2009).

34   Hellman, O., Abrikosov, I. A. & Simak, S. I. Lattice dynamics of anharmonic solids from first principles. *Physical Review B* **84**, 180301, doi:10.1103/PhysRevB.84.180301 (2011).

35   Hellman, O. & Abrikosov, I. A. Temperature-dependent effective third-order interatomic force constants from first principles. *Physical Review B* **88**, 144301, doi:10.1103/PhysRevB.88.144301 (2013).

36   Zhou, J.-J., Hellman, O. & Bernardi, M. Electron-Phonon Scattering in the Presence of Soft Modes and Electron Mobility in $SrTiO_3$ Perovskite from First Principles. *Physical Review Letters* **121**, 226603, doi:10.1103/PhysRevLett.121.226603 (2018).

37   Limonov, M. F., Rykov, A. I., Tajima, S. & Yamanaka, A. Raman scattering in $YBa_2Cu_3O_7$ single crystals: Anisotropy in normal and superconductivity states. *Physics of the Solid State* **40**, 367-376, doi:10.1134/1.1130327 (1998).

38   Maksimov, A. A. *et al.* Investigations of the temperature dependence of the low energy electronic Raman scattering in $Ti_2Ba_2CaCu_2O_8$ single crystals. *Solid State Communications* **81**, 407-410, doi:https://doi.org/10.1016/0038-1098(92)90767-4 (1992).

39   Panfilov, A. G., Limonov, M. F., Rykov, A. I., Tajima, S. & Yamanaka, A. Superconductivity-induced effect on "Raman-forbidden" modes in underdoped $YBa_2Cu_3O_{7-x}$ single crystals. *Physical Review B* **57**, R5634-R5637, doi:10.1103/PhysRevB.57.R5634 (1998).

40   Ashcroft, N. W. & Mermin, N. D. *Solid State Physics*. (Holt-Saunders, 1976).

41   Husmann, D. *et al.* Breakdown of the Wiedemann–Franz law in a unitary Fermi gas. *Proceedings of the National Academy of Sciences* **115**, 8563-8568, doi:doi:10.1073/pnas.1803336115 (2018).

42   Schabel, M. C. *et al.* Angle-resolved photoemission on untwinned $YBa_2Cu_3O_{6.95}$. I. Electronic structure and dispersion relations of surface and bulk bands. *Physical Review B* **57**, 6090-6106, doi:10.1103/PhysRevB.57.6090 (1998).

43   Uemura, Y. J. *et al.* Systematic variation of magnetic-field penetration depth in high-T_c superconductors studied by muon-spin relaxation. *Physical Review B* **38**, 909-912, doi:10.1103/PhysRevB.38.909 (1988).

44   Legros, A. *et al.* Universal *T*-linear resistivity and Planckian dissipation in overdoped cuprates. *Nature Physics* **15**, 142-147, doi:10.1038/s41567-018-0334-2 (2019).

45   Jorgensen, J. D. *et al.* Structural properties of oxygen-deficient $YBa_2Cu_3O_{7-\delta}$. *Physical Review B* **41**, 1863-1877, doi:10.1103/PhysRevB.41.1863 (1990).

46   Cava, R. J. *et al.* Structural anomalies, oxygen ordering and superconductivity in oxygen deficient $Ba_2YCu_3O_x$. *Physica C: Superconductivity* **165**, 419-433, doi:https://doi.org/10.1016/0921-4534(90)90376-P (1990).

47   Jorgensen, J. D. *et al.* Pressure-induced charge transfer and dT_c/dP in $YBa_2Cu_3O_{7-x}$. *Physica C: Superconductivity* **171**, 93-102, doi:https://doi.org/10.1016/0921-4534(90)90460-V (1990).

48   Torardi, C. C. *et al.* Structures of the superconducting oxides $Tl_2Ba_2CuO_6$ and $Bi_2Sr_2CuO_6$. *Physical Review B* **38**, 225-231, doi:10.1103/PhysRevB.38.225 (1988).

49   Yamamoto, A. *et al.* Rietveld analysis of the modulated structure in the superconducting oxide $Bi_2(Sr,Ca)_3Cu_2O_{8+x}$. *Physical Review B* **42**, 4228-4239, doi:10.1103/PhysRevB.42.4228 (1990).

50   Allen, S. M. & Thomas, E. L. *The Structure of Materials*. (Wiley, 1999).

51   Huang, Q. *et al.* Neutron powder diffraction study of the crystal structure of $HgBa_2Ca_4Cu_5O_{12+\delta}$ at room temperature and at 10 K. *Physica C: Superconductivity* **227**, 1-9, doi:https://doi.org/10.1016/0921-4534(94)90349-2 (1994).

52   Paranthaman, M. & Chakoumakos, B. C. Crystal Chemistry of $HgBa_2Ca_{n-1}Cu_nO_{2n+2+\delta}$($n=$ 1, 2, 3, 4) Superconductors. *Journal of Solid State Chemistry* **122**, 221-230, doi:https://doi.org/10.1006/jssc.1996.0105 (1996).

53   Loureiro, S. M. *et al.* Structure and superconductivity of the $HgBa_2Ca_3Cu_4O_{10+\delta}$ phase. *Physica C: Superconductivity and its Applications* **257**, 117-124, doi:https://doi.org/10.1016/0921-4534(95)00804-7 (1996).

54   Zandbergen, H. W. *et al.* Superconductivity in (Pb, $Bi)_2Sr_{2-x}La_xCu_2O_{6+\delta}$. *Physica C: Superconductivity* **159**, 81-86, doi:https://doi.org/10.1016/0921-4534(89)90107-X (1989).

55   Subramanian, M. A. *et al.* Superconductivity near liquid nitrogen temperature in the Pb-Sr-R-Ca-Cu-O system (R=Y or rare earth). *Physica C: Superconductivity* **157**, 124-130, doi:https://doi.org/10.1016/0921-4534(89)90477-2 (1989).

56   Subramanian, M. A. *et al.* Crystal structure of the high-temperature superconductor $TI_2Ba_2CaCu_2O_8$. *Nature* **332**, 420-422, doi:10.1038/332420a0 (1988).

57   Cox, D. E., Torardi, C. C., Subramanian, M. A., Gopalakrishnan, J. & Sleight, A. W. tructure refinements of superconducting $Tl_2Ba_2CaCu_2O_8$ and $Tl_2Ba_2Ca_2Cu_3O_{10}$ from neutron diffraction data. *Physical Review B* **38**, 6624-6630, doi:10.1103/PhysRevB.38.6624 (1988).

58   Cyr-Choinière, O. *et al.* Sensitivity of T_c to pressure and magnetic field in the cuprate superconductor $YBa_2Cu_3O_y$: Evidence of charge-order suppression by pressure. *Physical Review B* **98**, 064513, doi:10.1103/PhysRevB.98.064513 (2018).

59   Grover, T. & Fisher, M. P. A. Quantum disentangled liquids. *Journal of Statistical Mechanics: Theory and Experiment* **2014**, P10010, doi:10.1088/1742-5468/2014/10/p10010 (2014).

60   Eisert, J., Cramer, M. & Plenio, M. B. Colloquium: Area laws for the entanglement entropy. *Reviews of Modern Physics* **82**, 277-306, doi:10.1103/RevModPhys.82.277 (2010).

61   Bekenstein, J. D. Black Holes and Entropy. *Physical Review D* **7**, 2333-2346, doi:10.1103/PhysRevD.7.2333 (1973).

62   Hawking, S. W. Black hole explosions? *Nature* **248**, 30-31, doi:10.1038/248030a0 (1974).

63   Kresse, G. & Furthmuller, J. Efficiency of ab-initio total energy calculations for metals and semiconductors using a plane-wave basis set. *Computational Materials Science* **6**, 15-50 (1996).

64   Kresse, G. & Furthmuller, J. Efficient iterative schemes for ab initio total-energy calculations using a plane-wave basis set. *Physical Review B* **54**, 11169-11186 (1996).

65   Nosé, S. A unified formulation of the constant temperature molecular dynamics methods. *The Journal of Chemical Physics* **81**, 511-519, doi:10.1063/1.447334 (1984).

66   Hoover, W. G. Canonical dynamics: Equilibrium phase-space distributions. *Physical Review A* **31**, 1695-1697, doi:10.1103/PhysRevA.31.1695 (1985).

67   Vanderbilt, D. Soft self-consistent pseudopotentials in a generalized eigenvalue formalism. *Physical Review B* **41**, 7892-7895 (1990).

68   Perdew, J. P., Burke, K. & Ernzerhof, M. Generalized Gradient Approximation Made Simple. *Physical Review Letters* **77**, 3865-3868 (1996).

69   Grimme, S., Antony, J., Ehrlich, S. & Krieg, H. A consistent and accurate ab initio parametrization of density functional dispersion correction (DFT-D) for the 94 elements H-Pu. *The Journal of Chemical Physics* **132**, 154104, doi:10.1063/1.3382344 (2010).

Figures captions

Fig. 1: Phonon anomaly of the B_{1g} and A_g phonon modes.
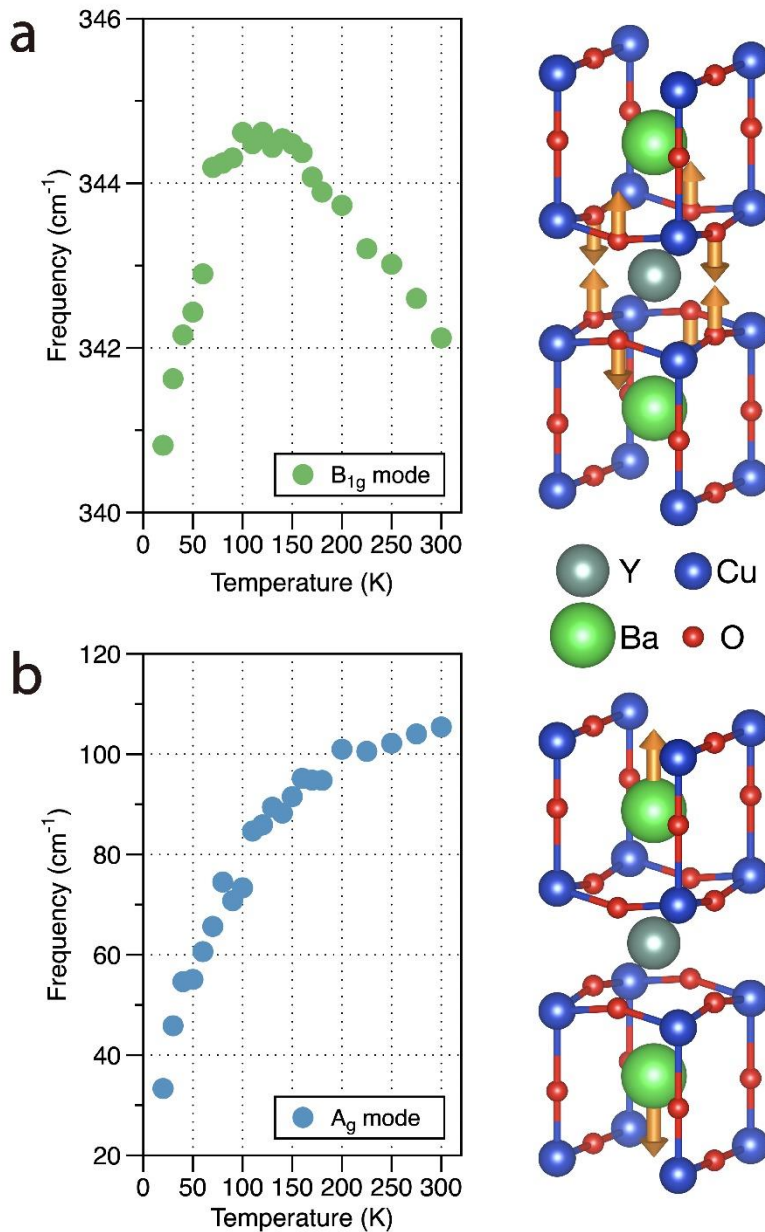
a, B_{1g} phonon frequency dependence on temperature. **b,** A_g phonon frequency dependence on temperature (left), and their corresponding phonon modes visualized with the orange arrows in the real-space lattice (right).

Fig. 2: Thermal decoupling from phonon dispersion and charge density analysis.
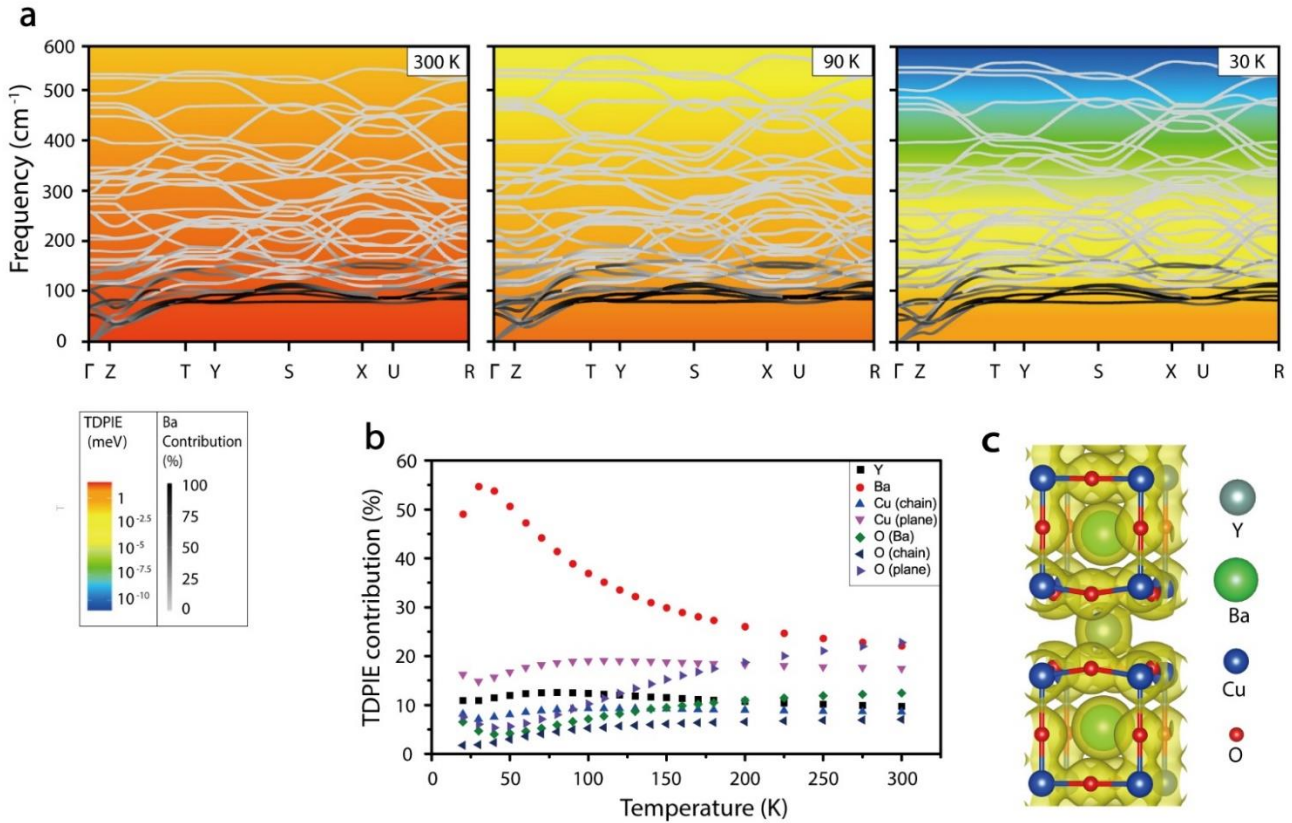
a, Phonon dispersions at 300, 90, and 30 K were calculated from the temperature-dependent effective potential. The colored backgrounds show the temperature-dependent part of internal energy (TDPIE) depending on the phonon frequency. The grayscale lines overlaying the phonon dispersion curves indicate the Ba contribution to each phonon mode evaluated by analyzing the phonon edge states. **b,** Contribution of each type of atom to TDPIE. The contribution of Ba increases as the temperature decreases. **c,** Charge density plot with the isosurface charge (0.047 electrons/a_0^3) exhibiting the electronic isolation of Ba atoms.

Fig. 3: Thermal decoupling of YBCO at low temperatures from *ab initio* molecular dynamics simulation.
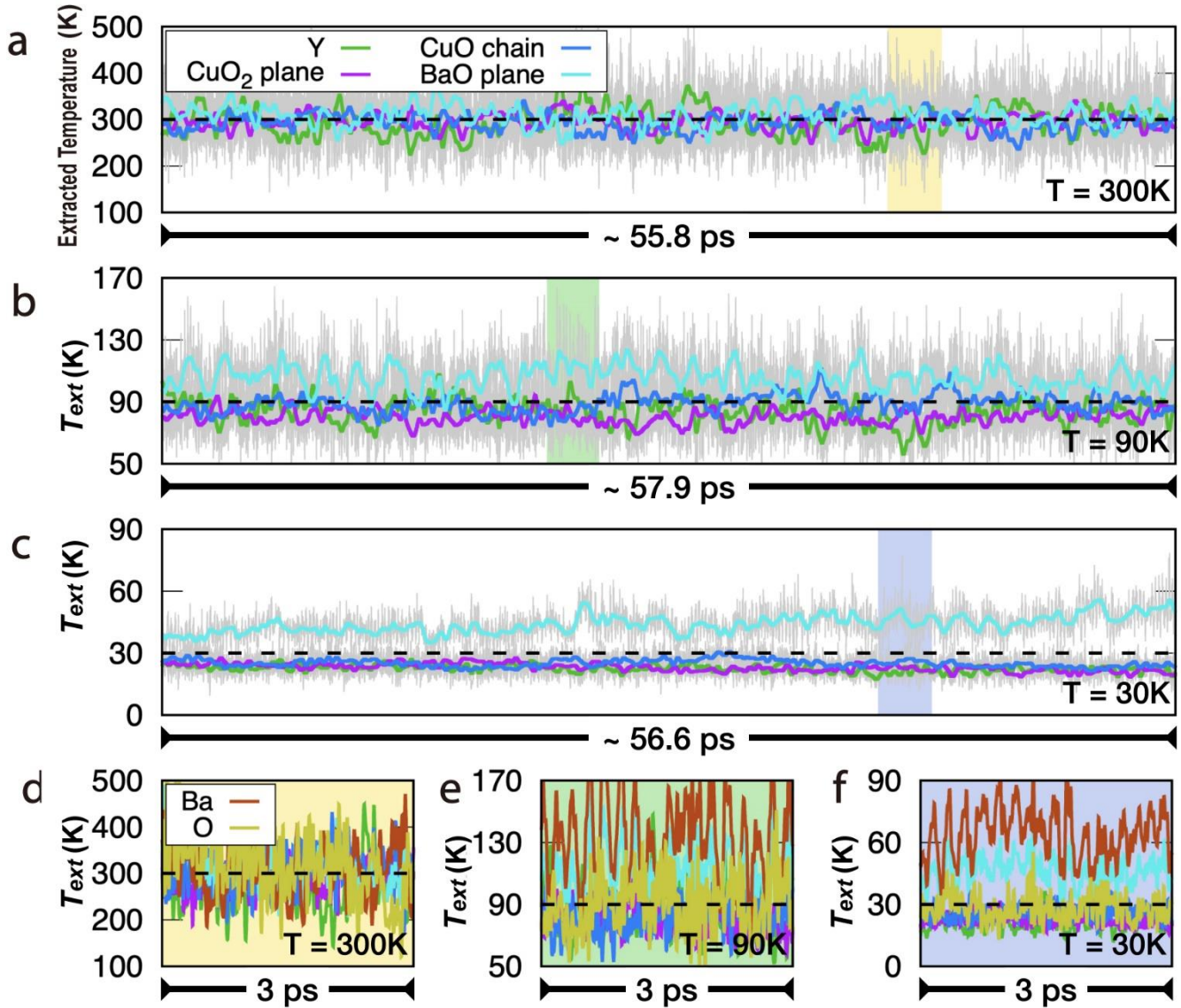
a-c, Layer-by-layer extracted temperatures (T_{ext}) at the system temperatures of 300, 90, and 30 K. **d-f,** Magnified view of T_{ext} of the Ba and O atoms in the BaO layer in the yellow, green, and violet regions in **a, b,** and **c,** respectively.

Fig. 4: BaO-plane temperature dependence of the B₁g phonon and the relationship between the temperatures of the CuO₂ and BaO planes.
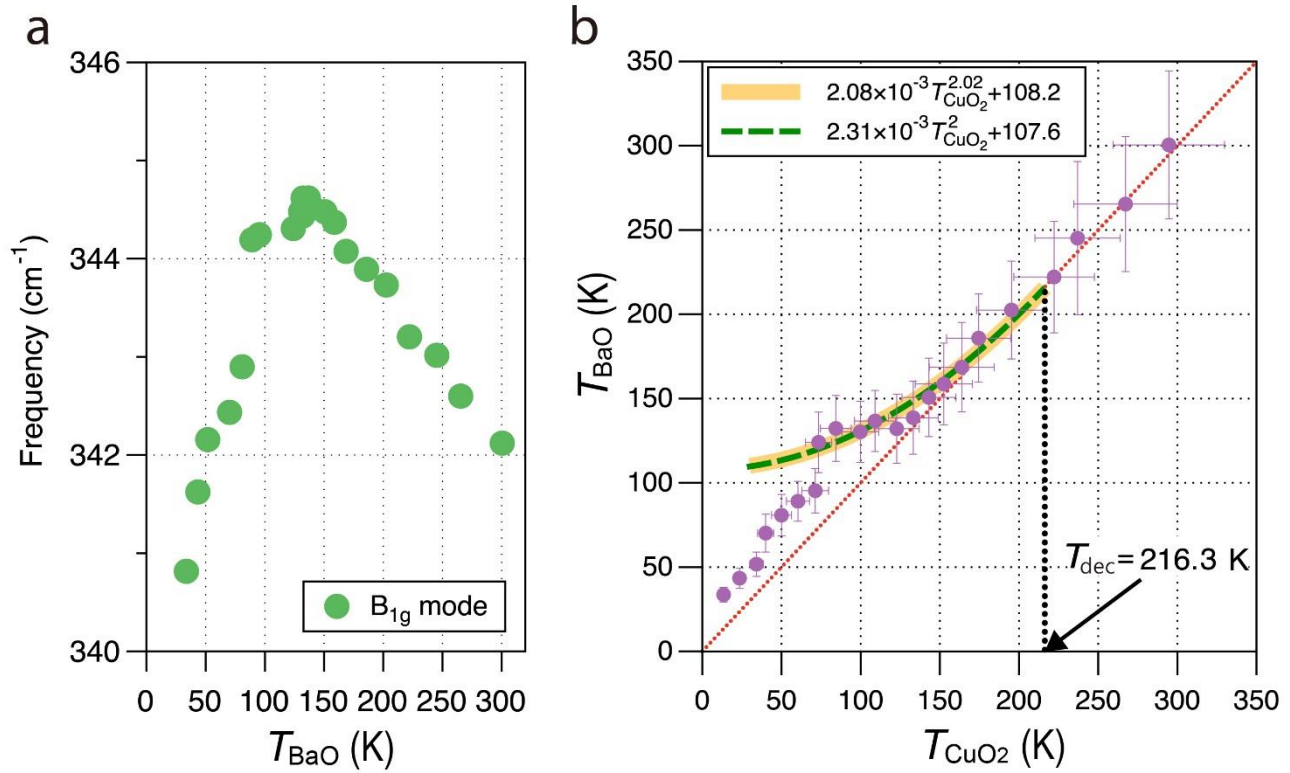
a, B1g phonon frequency as a function of the extracted temperature of the BaO plane (T_{BaO}). It shows the shift in temperature compared to Fig. 1a. **b,** The relationship between the extracted temperature of the CuO₂ plane (T_{CuO_2}) and the extracted temperature of the BaO plane (T_{BaO}). The fitting curves (thick yellow and dashed green lines) show the quadratic relation between T_{BaO} and T_{CuO_2}. The arrow and the number indicate the decoupling temperature (T_{dec}) between the BaO and the CuO₂ planes.

Fig. 5: Relationship between T_c and the Ba/Sr-CuO$_2$ plane distance in cuprates.
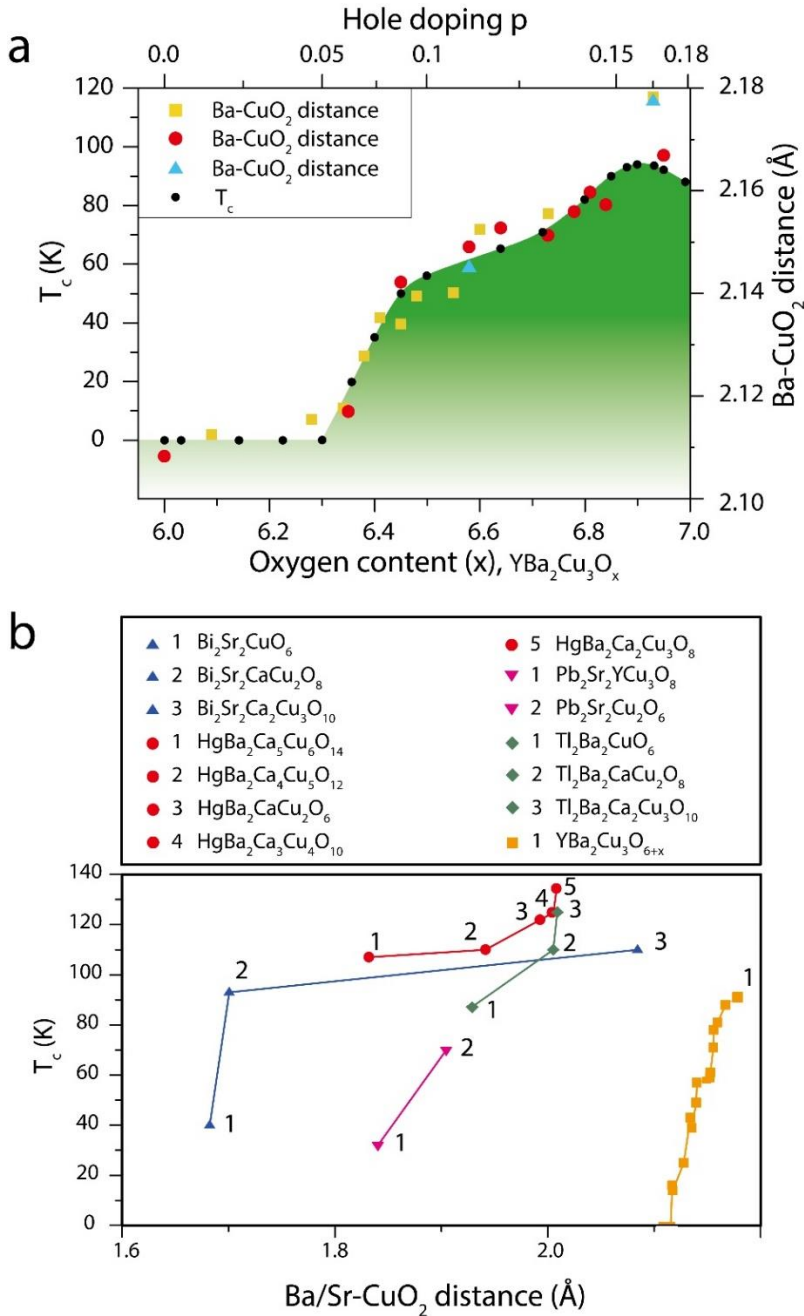
a, Distance between the Ba atom and the CuO$_2$ plane on the doping concentration of YBCO is well matched with T_c. Data for the distance between the Ba atom and CuO$_2$ plane extracted from three experimental measurements were marked with yellow squares[45], red circles[46], and blue triangles[47], respectively. **b,** The distance between the Ba or Sr atom and CuO$_2$ plane in various cuprate superconductors is matched with T_c. [48-57]

The English in this document has been checked by at least two professional editors, both native speakers of English. For a certificate, please see:

http://www.textcheck.com/certificate/7HuZTs